Electric Power Systems Research 104 (2013) 18–27

Contents lists available at ScienceDirect

Electric Power Systems Research

journal homepage: www.elsevier.com/locate/epsr

Short communication

A repetitive control system for four-leg matrix converters feeding non-linear loads

Roberto Cárdenas[a,*], Rubén Peña[b], Jon Clare[c], Patrick Wheeler[c], Pericle Zanchetta[c]

[a] University of Chile, Department of Electrical Engineering, Santiago, Chile
[b] University of Concepción, Department of Electrical Engineering, Concepción, Chile
[c] University of Nottingham, Department of Electrical and Electronic Engineering, Nottingham University Park, NG7 2RD Nottingham, England, United Kingdom

ARTICLE INFO

Article history:
Received 25 July 2012
Received in revised form 6 May 2013
Accepted 20 May 2013
Available online 7 July 2013

Keywords:
Repetitive control
Matrix converters
Generation systems

ABSTRACT

Generators working with variable speed, rather than fixed speed, have many advantages, which are well documented in the literature. Higher efficiency, better power to size ratio and less mechanical stress in the system are some of the characteristics of variable speed generators. In particular, variable speed diesel generators can be used to provide small highly portable generation systems for emergency vehicles and military/aerospace applications. Such systems can be used to feed stand-alone linear/non-linear loads if an adequate power converter interface is provided. Four-leg matrix converters can be used as the power electronic interface between variable speed generators and stand-alone loads. The fourth leg provides a neutral point for single phase loads and a path for the circulation of zero sequence currents. When non-linear loads are connected to the matrix converter output, relatively high harmonic distortion can be produced in the load voltage unless an appropriate control system is provided. In this paper the application of a repetitive control system to improve the quality of the load voltage is presented. Experimental results obtained from a prototype are shown and fully analysed.

1. Introduction

Conventional diesel generators have to be operated at fixed speed in order to supply the load with constant frequency [1]. However for light load operation the efficiency of such a system is low since the combustion process is poor and not all of the fuel is burned by the engine. This increases maintenance and operational costs [2–4]. Moreover, the diesel engine lifespan is reduced because the system has to be operated at a higher average temperature. To avoid this problem, variable speed operation of diesel generators has been proposed in the literature [2–4]. There are at least two important advantages related to the variable speed operation of diesel engines:

- The fuel consumption can be substantially reduced [2]. As reported in previous publications [2,3,5], when the diesel generator is operated along an optimal power-speed locus, the diesel engine efficiency is increased.
- A small portable generation system can be implemented [1,2,6]. Virtually all diesel engines of interest (especially lightweight automotive engines) are designed for sustained operation at rotational speeds much higher than 1500 rpm and can produce much more power if allowed to operate at higher speeds [7]. Limiting operation to 1500 rpm effectively de-rates the engine.

Load adaptive variable-speed diesel technology increases the portability of the generation system. It adapts to any load and changes the speed to the most efficient point for a given electrical power consumption. A much smaller less expensive technology, such as engines designed for automotive applications, can be used.

1.1. Power converters for variable speed generation

When a variable speed generator is used to supply electrical energy to isolated loads, power converter interfaces have to be provided to supply constant frequency and voltage at the output. If star-connected unbalanced stand-alone loads are present, then a neutral connection has to be provided in order to supply a path for the circulation of zero sequence current. In some applications the generator is connected to a bridge rectifier and a 3-leg voltage source inverter (VSI) at the output [1,2]. For this topology a

* Corresponding author at: University of Chile, Avenida Tupper 2007, Postcode 8370451, Chile. Tel.: +56 2 9784816; fax: +56 2 6720162.
E-mail addresses: rcd@ieee.org, rcardenas@ing.uchile.cl (R. Cárdenas), rupena@udec.cl (R. Peña), jon.clare@nottingham.ac.uk (J. Clare), pat.wheeler@nottingham.ac.uk (P. Wheeler), pericle.zanchetta@nottingham.ac.uk (P. Zanchetta).

0378-7796/$ – see front matter © 2013 Elsevier B.V. All rights reserved.
http://dx.doi.org/10.1016/j.epsr.2013.05.012

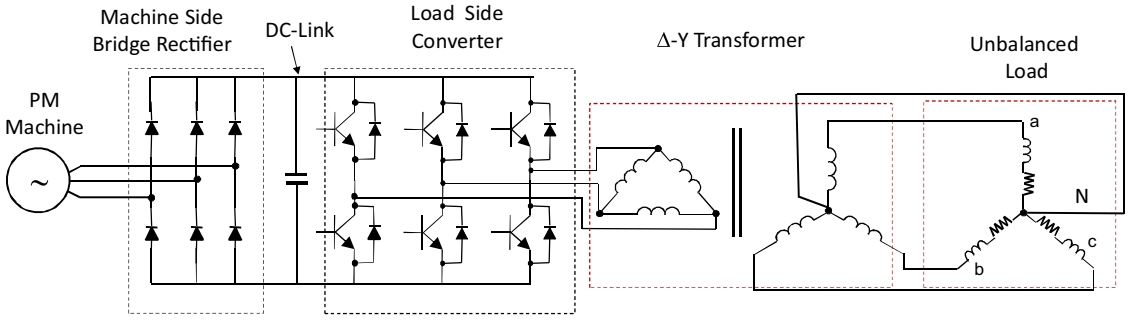

Fig. 1. Variable speed generation system feeding an unbalanced stand-alone load.

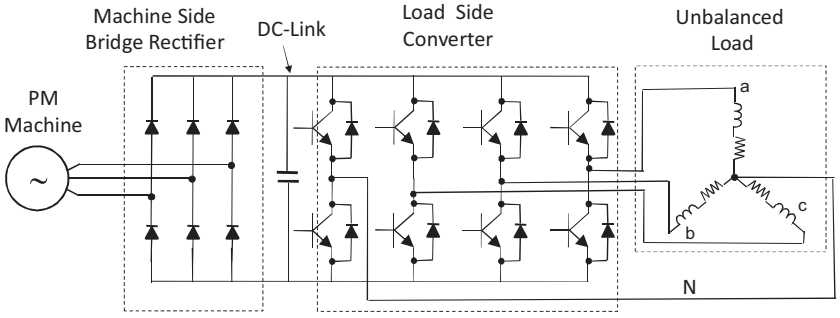

Fig. 2. Variable speed generation system employing a 4-leg VSI.

Δ-Y power transformer is connected to the VSI, providing a path for the circulation of the zero sequence current (see Fig. 1). This bulky transformer can be avoided if a 4-leg voltage source inverter is used as shown in Fig. 2. In this case one of the legs of the load-side converter is controlled to provide the neutral connection to the load. To increase the operating speed range, the bridge rectifier can be replaced by a 3-leg VSI. In that case two VSIs are required in a back-to-back topology implemented with seven legs, three at the generator-side converter and four at the load side converter (see Fig. 2).

When portability is important, for instance to provide a generation system which can be used in an emergency vehicle [1,2,7] or aerospace applications [8], the 7-leg back-to-back converter can be replaced by a 4-leg matrix converter (MC) [9,10]. Again, the fourth leg of the MC is provided to allow the circulation of zero sequence currents in the load.

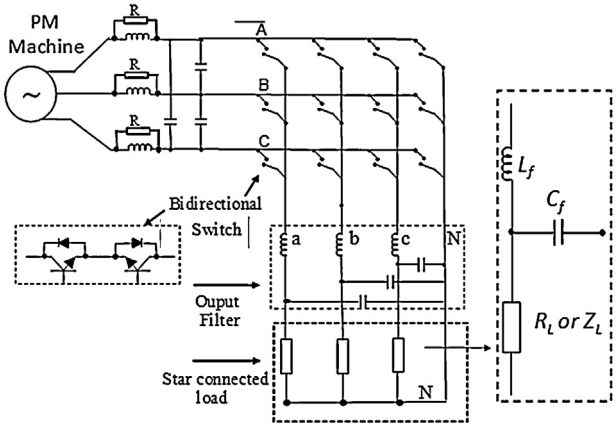

Fig. 3. A 4-leg matrix converter.

1.2. 4-Leg matrix converters

The main advantages of MCs are the size, portability, reliability and efficiency [11,12]. Because the dc-link capacitors are eliminated from the topology, the reliability is increased [11] and a much better power to size ratio is obtained with respect to that of conventional back-to-back converters. This is discussed in [12]. As reported in that publication for a given nominal power and depending on the switching frequency, the MC volume can reduce to only about one-third/one-fifth of the volume of a VSI-based back-to-back converter, achieving a better overall efficiency. Moreover, the MC can be embedded in the stator of the generator as reported in [13].

Fig. 3 shows a 4-leg MC connected to a permanent magnet (PM) generator at the input. The 4-leg MC is feeding a stand-alone load at the output. A filter is used to reduce the total harmonic distortion (THD) in the input current and it also provides the decoupling capacitors required for current commutation. Twelve bidirectional switches are used in the converter, each one composed of two IGBTs and two diodes. Typically the switching of the IGBTs in each bidirectional switch is controlled using the 4-step commutation method to avoid the momentary disconnection of the inductive load connected at the matrix converter output [14,15]. A second order LC filter is required to reduce the distortion in the load voltage. The design of this filter is conventional and the cut-off frequency has to be selected in order to adequately attenuate the switching harmonics, without affecting the 50 Hz components.

Space vector modulation is well known for conventional 3×3 matrix converters and its implementation and desirable characteristics have been widely discussed in the literature [33]. In this work, we use the only extension of the SVM method reported for the 3×4 case [9,10] where the MC output vectors are represented in the three-dimensional α–β–γ space. Further details about the modulation algorithm are considered outside the scope of this paper and the interested reader is referred elsewhere [9,10].

Fig. 4 shows the variable speed diesel generation system proposed in this work. The system is controlled using a DSP + FPGA based control platform. The FPGA is used in the implementation of the SVM, 4-step commutation method [15] and control of the A/D–D/A converters. A 4-leg MC is connected to the generator to

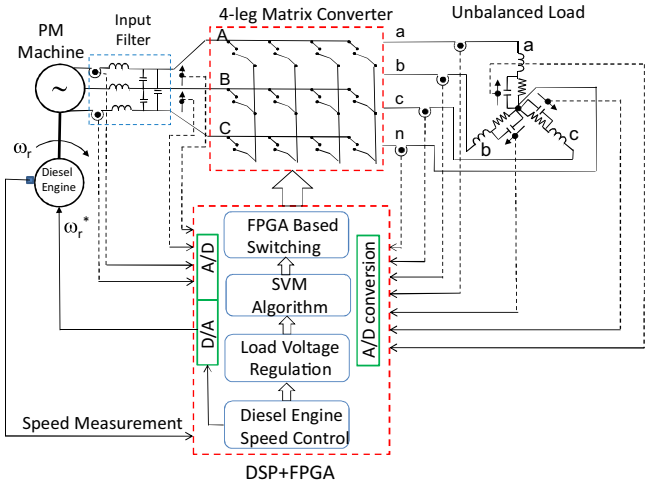

Fig. 4. Variable speed generation system proposed in this work.

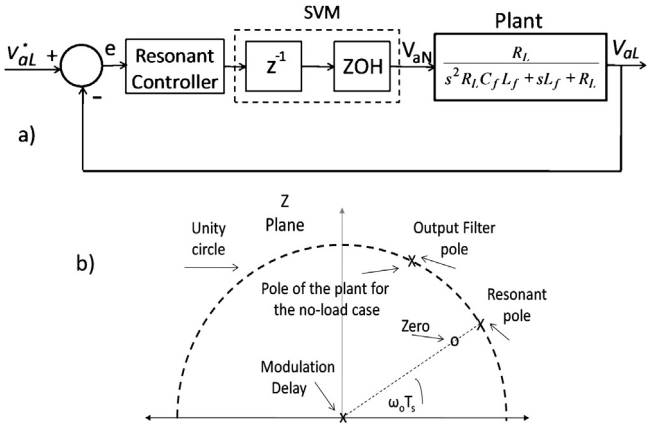

Fig. 5. Resonant control system. (a) Closed loop system. (b) Pole-zero placement of (2) in the *Z* plane.

feed the unbalanced load. The rotational speed of the diesel generator is controlled in order to operate the engine along the optimal power characteristic [3].

When non-linear loads are connected to the matrix converter output, relatively high harmonic distortion can be produced in the load voltage unless an appropriate control system is provided. In this paper the application of a repetitive control system to improve the quality of the load voltage fed by a variable speed system is presented in Section 2.

The rest of this paper is organised as follows. In Section 2 repetitive and resonant controllers are discussed. The design and implementation of the control system is presented in Section 3. In Section 4 the input current distortion is briefly analysed. Experimental results are fully discussed in Section 5. Finally an appraisal of the work is presented in Section 6.

2. Repetitive control system

The variable speed generation system of Fig. 4 can be used to feed non-linear loads. In this case the load voltages can have a relatively high harmonic distortion unless an appropriate control system is used. To deal with this situation the use of resonant controllers for 3×4 MC applications has been reported in [5,16,17]. In the Laplace plane a resonant controller has two purely imaginary poles with a resonant frequency of ω_o, where ω_o is the desired output frequency. A resonant controller, implemented in *a-b-c* natural coordinates, has the following transfer function:

$$G_c(s) = K_c \frac{s^2 + 2\zeta\omega_n s + \omega_n^2}{s^2 + \omega_0^2} \tag{1}$$

where K_c is the controller gain. In the numerator of (1), zeros located close to the resonant poles are used to improve the dynamic response. Fig. 5a shows the implementation of the resonant controller for the regulation of a single harmonic component of frequency ω_0. In this graphic υ_{aL}^* is the reference voltage for the load voltage in phase "*a*" with respect to the neutral connection "*N*" and υ_{aN} is the voltage at the output of the MC. Notice that in Fig. 5a the space vector modulation algorithm is represented by a one sample time delay plus a zero order hold (ZOH). At the output of the plant (see (7)) the voltage υ_{aL} is measured and fed back to the control system.

In the z-plane, the transfer function of the resonant controller is:

$$G_c(z) = K_{cz} \frac{z^2 + a_1 z + a_2}{z^2 + b_1 z + b_2} \tag{2}$$

In this case the resonant poles are located on the unit circle, as shown in Fig. 5b, making an angle with respect to the real axis of $\omega_0 T_s$ rad s^{-1}, where T_s is the sampling time. Notice that the digital implementation of (2) requires at least five floating point multiplications plus some additions and memory storage operations. Using the internal model principle [18] it is relatively simple to demonstrate that the resonant controller of (1) regulates any signal of frequency ω_0 in the load voltage with zero steady state error. However if the load current is distorted, a high order resonant controller is required in order to regulate the harmonic voltage components that are otherwise generated. This regulator has the following transfer function:

$$G_c(s) = K_{c1} \frac{s^2 + 2\zeta\omega_{n1} s + \omega_{n1}^2}{s^2 + \omega_{o1}^2} + K_{c2} \frac{s^2 + 2\zeta\omega_{n2} s + \omega_{n2}^2}{s^2 + \omega_{o2}^2} + \ldots + K_{cm} \frac{s^2 + 2\zeta\omega_{nm} s + \omega_{nm}^2}{s^2 + \omega_{om}^2} \tag{3}$$

where each resonant controller has a gain K_{ci}, a resonant frequency ω_{oi} and two complex zeroes designed to increase the stability of the system. Using the controller of (3) output signals with frequencies of ω_{oi} can be independently regulated or eliminated from the output.

Control systems based on multiple resonant controllers have already been reported in [17] where the performance of a control algorithm with six resonant controllers per phase, tuned at 0 Hz, 50 Hz, 100 Hz, 150 Hz, 200 Hz and 250 Hz, is discussed. The performance of that controller is good with a fast dynamic response. As discussed in [17], for a non-linear load the total harmonic distortion can be reduced from 15% to 3%. However the computational burden required for implementing eighteen resonant controllers in each sampling time is high and the switching frequency of the MC had to be reduced from 10 kHz to 5 kHz in [17]. This is undesirable since one of the main advantages of MCs, their good power to size ratio [13,19], is lost when the switching frequency is reduced due to the need for bigger filters [19].

Repetitive control systems [20–23] are an alternative to resonant controllers and are based on a similar principle, i.e. to use resonant poles in order to regulate or eliminate signals of frequencies ω_{oi} [18]. The repetitive controller achieves this efficiently, since its transfer function typically requires low processing power for digital implementation [24,25].

Repetitive controllers are based on the equation: $Z^N - 1 = 0$ which produces *N* roots located on the unit circle in the z-plane. The equation can be solved using:

$$Z^N - 1 = 0 \Rightarrow \text{angle}(Z^N) = 0 \tag{4}$$

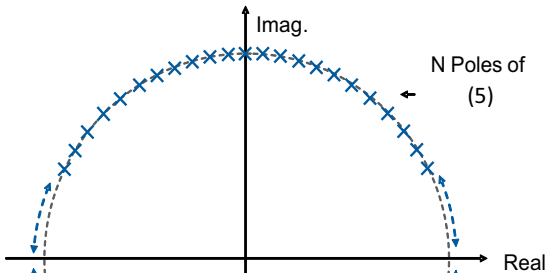

Fig. 6. Poles of (5) on the unit circle in the *z*-plane.

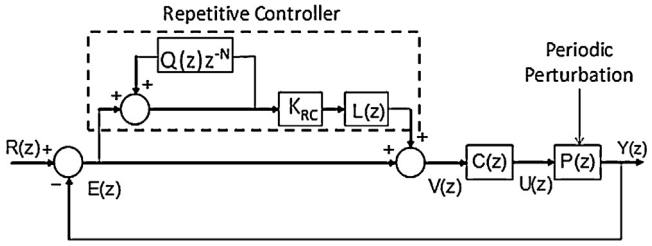

Fig. 7. Repetitive control system.

Using (4) it is relatively simple to demonstrate that control systems with the transfer function:

$$G_c(z) = \frac{k_{cz}}{1 - z^{-N}} \tag{5}$$

Have *N* poles located on the unit circle, as shown in Fig. 6. Therefore, *N* resonant poles are produced by (4) and (5) whose expressions are simpler than the high order controller of (3). Repetitive controllers are also based on the internal model principle [18] and are mainly used to eliminate the effect of harmonics in closed loop systems [20,21].

If an unbalanced non-linear load is connected to the system output (see Fig. 5a), the harmonic distortion produced in the voltage can be represented as sinusoidal signals with frequencies $k\omega_o$ where ω_o is the output fundamental frequency and k is an integer. Therefore the harmonic distortion can be considered a periodic perturbation to be eliminated by the repetitive controller. The value of N in (5) is an integer equal to ω_s/ω_o, where ω_s is the sampling frequency. The controller of (5) cannot be used directly in the closed loop control system because the N open loop poles located along the unit circle may reduce the phase margin of the system below an acceptable value. Therefore some additional compensators have to be added to (5) in order to improve the phase margin of the control loop [29].

Fig. 7 shows the repetitive control system proposed in this paper. The design of the repetitive controller and additional lead compensators is based on the design procedure reported in [26]. The "plug in" topology reported in [23,26] has been selected because it allows a simple implementation where the repetitive controller augments the conventional controller $C(z)$ (see [16,26]). Other repetitive controller topologies are also possible [30–32], but they are not considered further here.

In Fig. 7 the transfer function $Q(z)$corresponds to a zero phase-shift, low-pass filter with transfer function [26]:

$$Q(z) = \frac{\gamma_p(z^{-p} + z^{p}) + \gamma_{p-1}(z^{-(p-1)} + z^{p-1}) + \cdots + \gamma_0}{2\gamma_p + 2\gamma_{p-1} + \cdots + \gamma_0} \tag{6}$$

where $\gamma_0 > \gamma_1 > \cdots > \gamma_p$. The low pass filter $Q(z)$ is used to reduce the high frequency gain of the repetitive controller, increasing the stability of the system. A zero phase-shift transfer function for $Q(z)$ is recommended in [26] in order to avoid reduction in the system phase margin. Other transfer functions, suitable for the implementation of $Q(z)$, are discussed in [26,30–32].

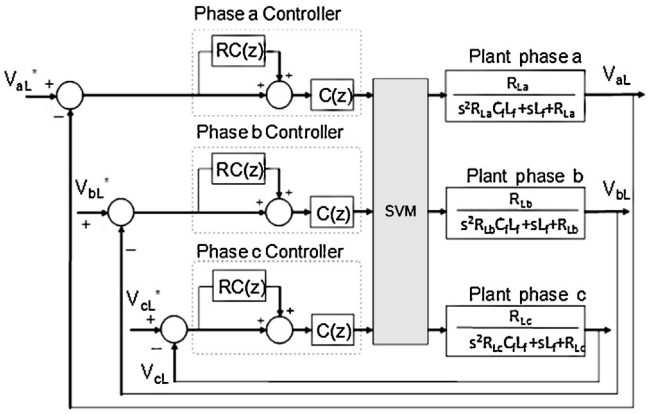

Fig. 8. Three phase control system including the repetitive control topology of Fig. 2.

Transfer function $P(z)$ corresponds to the plant connected at the MC output. With an unbalanced linear load (see Fig. 8) the plant can be different in each phase, i.e. it can be represented as three transfer functions $P_a(z)$, $P_b(z)$ and $P_c(z)$. Assuming a resistive load connected at the MC output (see Figs. 5a and 8), the plant $P_a(s)$ can be represented as:

$$P_a(s) = \frac{V_{aL}}{VaN} = \frac{R_{La}}{s^2 R_{La} C_f L_f + sL_f + R_{La}} \tag{7}$$

where V_{aN} is the line to neutral voltage of phase "a" at the MC output and V_{aL} is the load voltage. The transfer functions $P_b(s)$and $P_c(s)$ are obtained by replacing R_{La} with R_{Lb} and R_{Lc} respectively. For simplicity, resistive loads have been assumed. Furthermore, for design purposes it is assumed that the load resistance $R_L \to \infty$. This is the worst case situation corresponding to a damping factor of zero in the output stage. If the load resistance is decreased, the output filter pole shown in Fig. 5b moves inside the unit circle increasing the dynamic stability of the control system.

In Fig. 7, the signal $U(z)$ is the demanded voltage which is the input to the three dimensional SVM algorithm, designed for 4-leg matrix converters, and reported in [10]. $L(z)$ is a lag network used to reduce the high frequency gain of the repetitive control system and K_{rc} corresponds to the gain of the repetitive controller. As mentioned before, the value of N (see Fig. 7) is an integer corresponding to the ratio between the sampling frequency and the MC output fundamental frequency. A block diagram considering the three repetitive controllers, to regulate each phase to neutral voltage, is shown in Fig. 8 (where "*RC*" denotes repetitive controller). In this case, given the design assumptions, the three controllers are identical. For simplicity, in Fig. 8 the transformation from a–b–c to α–β–γ and vice versa are considered as part of the block labelled "SVM" and the MC is considered ideal, such that the demanded voltages are reproduced exactly at the converter output.

3. Control system implementation

The generation system shown in Fig. 3 has been implemented using a second order output filter with $L_f = 2.5$ mH and $C_f = 40$ μF. The sampling time is 100 μs, for a switching frequency of 10 kHz and the MC output frequency is 50 Hz. In the *z*-plane, the transfer function of the repetitive controller is:

$$RC(z) = \frac{K_{RC} \cdot L(z)}{1 - Q(z) \cdot z^{-N}} \tag{8}$$

where $N = 200$. Considering the stability analysis presented in [26] a K_{RC} value of 1 has been selected in this work. As explained before

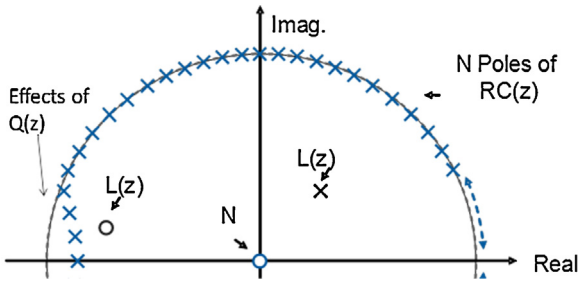

Fig. 9. Poles and zeroes for the transfer function of (8)–(11).

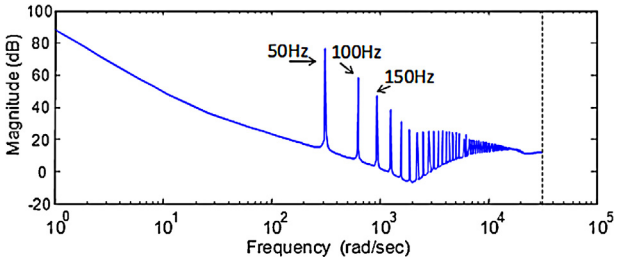

Fig. 10. Bode diagram of the proposed controller.

$Q(z)$ is used to reduce the high frequency gain of the repetitive controller. An additional degree of freedom to compensate for the high frequency gain is provided by the transfer function $L(z)$ see [26,30–32].

Satisfactory results have been obtained employing the following transfer functions for $L(z)$ and $Q(z)$:

$$Q(z) = \frac{z^{-1} + 2 + z}{4} \tag{9}$$

$$L(z) = \frac{0.195z^2 + 0.3895z + 0.1948}{z^2 - 0.4833z + 0.2522} \tag{10}$$

which have been analysed and tuned using the RLTOOL command available in MATLAB® control-toolbox software. The root locus method, combined with Bode diagrams [29], has been used in the analysis of the proposed control system (see (8)). The design aims are to place all the closed loop poles inside the unit circle in the z-plane with a phase margin of at least 40–45° for the open loop transfer function of Fig. 7 (considering compensators and plant). A computer model of the system that considers all the digital effects and the space vector modulation algorithm was implemented in SIMULINK®. This model was used to verify the expected performance of the proposed controller in advance of the experimental implementation.

The poles and zeroes for the transfer function of (8) are shown in Fig. 9, illustrating the N poles and N zeroes produced by the repetitive control system. In Fig. 9, the high frequency poles, located close to $f_s/2$ (where f_s is the sampling frequency), are not on the unit circle because of the influence of the low pass filter $Q(z)$ and the lag network $L(z)$ in (8). The function of the lag transfer function $L(z)$, is to reshape the root locus, reducing the high frequency gain of the repetitive control system. The transfer function of (9) corresponds to the zero phase-shift, low-pass filter employed.

In Figs. 7 and 8, the transfer function $C(z)$ corresponds to a conventional PI controller cascaded with a lead-lag network. The PI controller is required to eliminate any dc component from the load voltage. Such dc components are typically produced by some non-linear loads, e.g. half-wave rectifiers. The transfer function $C(z)$ used is:

$$C(z) = 3 \cdot \frac{z - 0.8283}{z - 1} \cdot \frac{z^2 - 1.868z + 0.9049}{z^2 - 1.214z + 0.37} \tag{11}$$

The term to the left of (11) corresponds to the z-plane PI controller. Notice that the transfer function of (8) already has a pole at $z = 1$ [31,32]. However, for the transfer functions of (9)–(11) the term $1 + RC(z)$ (see Fig. 7) has a zero located very close to $z = 1$, almost cancelling the aforementioned pole (note that this pole-zero cancellation effect is located within the digital controller, and is not affected by plant parameter variations).Therefore an additional integrator has been included in (11) in order to increase the dc-gain of the controller.

The second order transfer function at the right of (11) is a lead-lag compensator which is used mainly to compensate for the oscillatory behaviour due to the open loop poles of the LC output filter. This lead-lag network can be also used to increase the phase margin of the entire system. A Bode diagram for the proposed controller (see (8)) is shown in Fig. 10. Notice the high gain peaks at integer multiples of the fundamental frequency. As depicted in Fig. 10, the high frequency gain has been significantly reduced.

4. Input current waveform

One of the applications of the four-leg matrix converter based system (see Figs. 3 and 9) is to feed non-linear loads. Since the matrix converter does not have energy storage components [14], instantaneous power balance between the input and the output of the converter can be used to calculate the harmonic components in the input current.

Assuming that the MC output currents and voltages are unbalanced and contain components at frequencies "ω_0" and "$n\omega_0$", then the instantaneous output power is:

$$P_0 = \frac{2}{3} Re\left[(\upsilon_1 e^{j\omega_0 t} + \upsilon_2 e^{-j\omega_0 t} + \upsilon_{n1} e^{jn\omega_0 t} + \upsilon_{n2} e^{-jn\omega_0 t})(i_1 e^{j(\omega_0 t + \theta_1)} + i_2 e^{-j(\omega_0 t + \theta_2)} + i_{n1} e^{j(n\omega_0 t + \theta_{n1})} + i_{n2} e^{-j(n\omega_0 t + \theta_{n2})})^c\right] \tag{12}$$

where the subscripts "1", "2" stand for positive and negative sequence components respectively. The superscript "c" stands for the complex conjugate operator and θ_1, θ_2, θ_{n1}, and θ_{n2} are arbitrary phase angles. Assuming that the input voltage is balanced, the input power is:

$$P_i = P_0 = \frac{2}{3} Re(\underline{\upsilon}_i \underline{i}_i^c) \tag{13}$$

Using (12) in (13) yields:

$$Re(\underline{i}_i) = \frac{2}{3} Re\left[\begin{array}{c} e^{-j\omega_i}(\upsilon_1 e^{j\omega_0 t} + \upsilon_2 e^{-j\omega_0 t} + \upsilon_{n1} e^{jn\omega_0 t} + \upsilon_{n2} e^{-jn\omega_0 t}) \\ \hline \frac{(i_1 e^{-j(\omega_0 t + \theta_1)} + i_2 e^{j(\omega_0 t + \theta_2)} + i_{n1} e^{-j(n\omega_0 t + \theta_{n1})} + i_{n2} e^{j(n\omega_0 t + \theta_{n2})})}{|\underline{\upsilon}_i|} \end{array}\right] \tag{14}$$

Using (14) it is relatively simple to conclude that the input current has frequency components of order ω_i, $(\omega_i - 2\omega_o)$, $(\omega_i + 2\omega_o)$, $\omega_i + (n-1)\omega_o$, $\omega_i - (n-1)\omega_o$, $\omega_i + (n+1)\omega_o$, $\omega_i - (n+1)\omega_o$, $(\omega_i - 2n\omega_o)$ and $(\omega_i + 2n\omega_o)$. Even if the load is unbalanced containing only positive and negative sequence current components, harmonic distortion with frequencies of $(\omega_i - 2\omega_o)$ and $(\omega_i + 2\omega_o)$ will be present at the MC input current. More information about input current distortion of 4-leg MCs is available elsewhere [10,16,17].

The current distortion, due to output unbalance, is handled by the generator, which is usually capable of operating with significant current waveform distortion [8,27,28]. Nevertheless, local heating or relatively large torque pulsations might be produced if the THD in the MC input current is too large. In a practical system there will

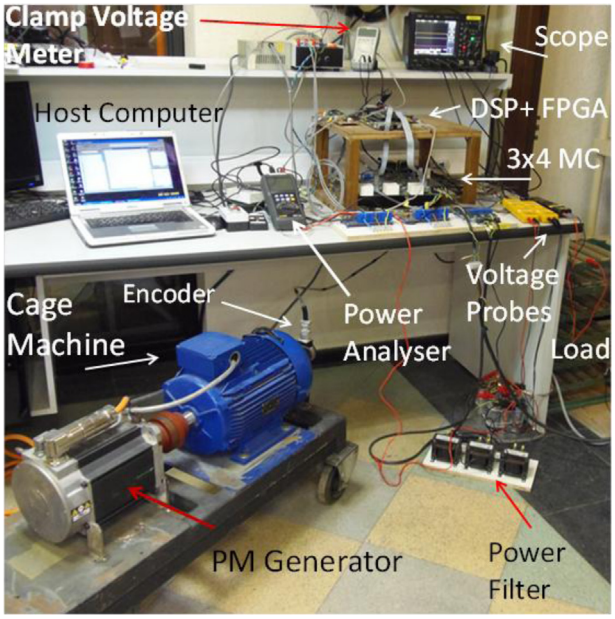

Fig. 11. Experimental system.

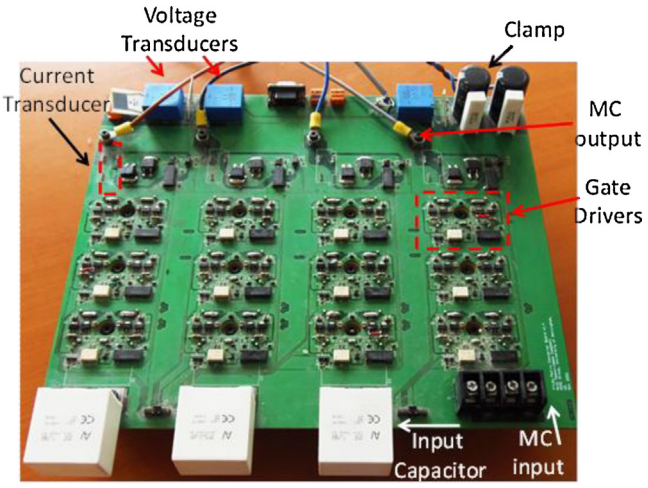

Fig. 12. 3 × 4 MC used in this work.

ultimately be a limit to the degree of input current distortion that can be tolerated [10].

5. Experimental results

The control methodology discussed in this work has been validated using the experimental system shown in Fig. 11. The SVM algorithm and repetitive control systems are implemented using a DSP based control board and an FPGA, the latter implementing the four-step commutation method and generating the switching signals for the IGBT gate drivers [15]. Either a three-phase variable transformer or a PM generator can feed the MC input. For data acquisition an external board, with 10, 14 bit, analogue to digital (ADC) channels (1 μs conversion time), is interfaced to the DSP. Data acquisition is also realised using a digital oscilloscope with a maximum storage capability of 500 k points and a maximum sampling rate of 2 GS/s. Hall-effect transducers are used to measure the input and output currents and voltages. A single-phase power quality analyser has also been used to measure the harmonic distortion in the currents and load voltages. Hall effect current probes with a bandwidth of 2 MHz are used to measure the currents. For the measurements of the voltage signals, differential probes of 25 MHz bandwidth are used. More information about the experimental system is given in Appendix.

Fig. 12 shows the 3 × 4 phase MC prototype used in this work. The MC was designed by the Power Electronic Machines and Control Group (PEMC) at the University of Nottingham. It uses 12 bidirectional switches, type Semikron SK60GM123, and includes a clamp circuit and 4 current/3 voltage transducers.

Steady state performance of the repetitive controller, obtained from the digital oscilloscope, is shown in Fig. 13. For this test a star connected load is used. The fourth leg of the MC is connected to the load neutral (see Fig. 3). Resistive loads of approximately 15 Ω are connected between the neutral point and phases *b* and *c*. In phase *a*, the 15 Ω resistive load is connected in series with a diode rectifier. A 70 V 50 Hz three-phase reference voltage signal is internally generated by the DSP.

Fig. 13a shows the waveforms corresponding to open loop operation. The distortion is high in V_{an} with a total harmonic distortion (THD) close to 9%. Some distortion is also present in the waveforms corresponding to V_{bn} and V_{cn}. Notice that the waveforms shown

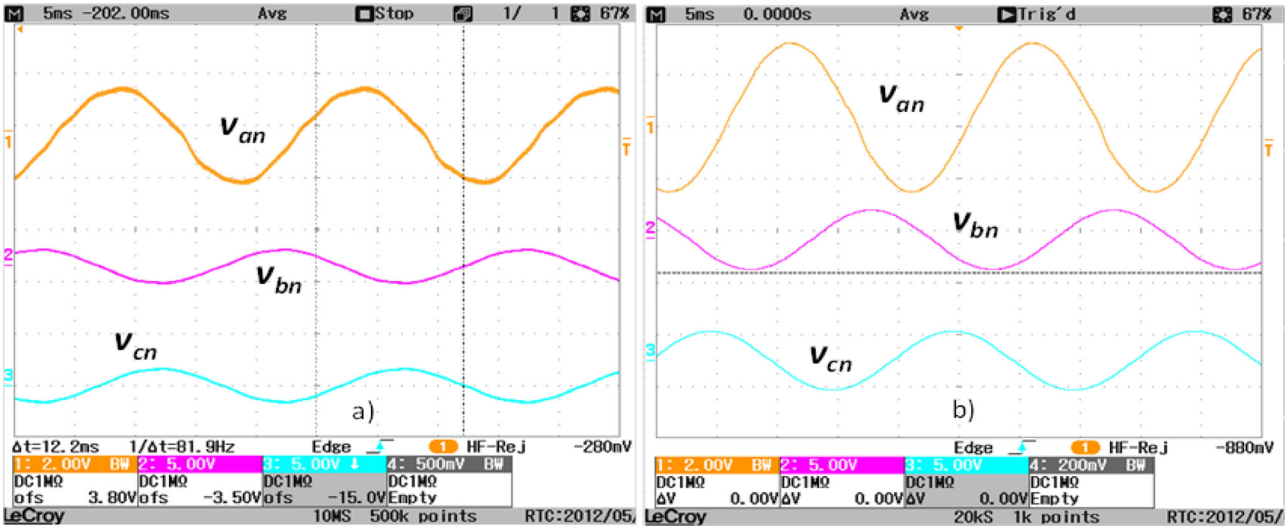

Fig. 13. Steady-state performance of the repetitive controller. (a) Load voltage waveforms corresponding to open-loop operation. (b) Load voltage waveforms corresponding to closed-loop operation of the repetitive controller.

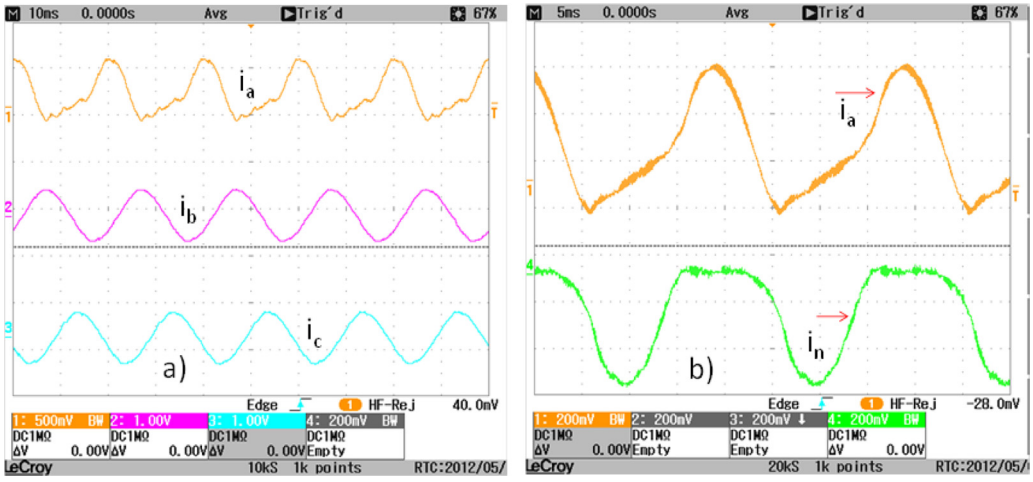

Fig. 14. Steady-state performance of the repetitive controller. (a) MC output currents i_a, i_b, i_c. (b) Matrix converter output current i_a and the neutral current i_n.

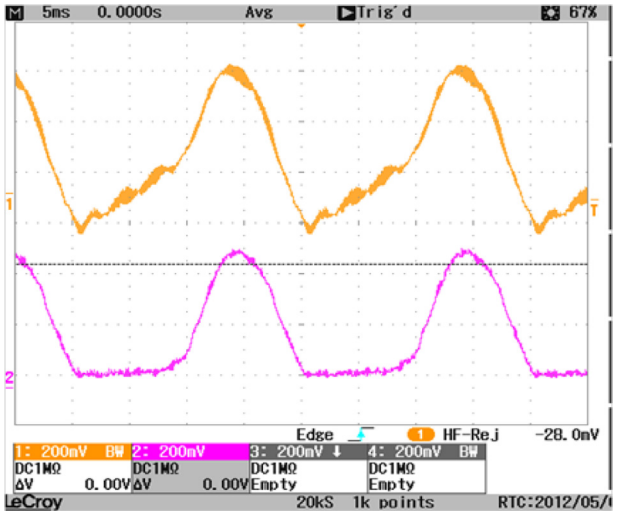

Fig. 15. MC output current i_a and the load current i_L.

in Fig. 13a have a dc component of about 7% of the fundamental voltage due to the half wave rectification in phase *a*.

Closed loop operation of the proposed repetitive controller is shown in Fig. 13b, in this case a THD of about 2.4% is achieved for V_{an}. This is a good improvement over the value obtained for open loop operation. The repetitive control routine requires only 50 μs of processing time in the DSP (Texas Instruments TMS320C6713). As shown in Fig. 13b, the waveforms corresponding to V_{bn} and V_{cn} are almost distortion free. For the experimental test corresponding to Fig. 13, a gain of 1/20 has been set in the differential voltage probes in order to measure the phase to neutral load voltages. The difference between the voltages of Fig. 13a and Fig. 13b are due to the fact that in Fig. 13a the voltage drops in the devices, output filter and matrix converter gain variations are not compensated by the control system.

In Fig. 14 the MC output currents corresponding to Fig. 13 are shown. The current is measured with a voltage to current ratio of 100 mV/A. Fig. 14a shows the currents in the MC outputs *a*,*b*,*c*. The current i_a has very high distortion with a THD of 43%. Notice that i_a has a dc current component which circulates through the fourth leg. This is shown in Fig. 14b.

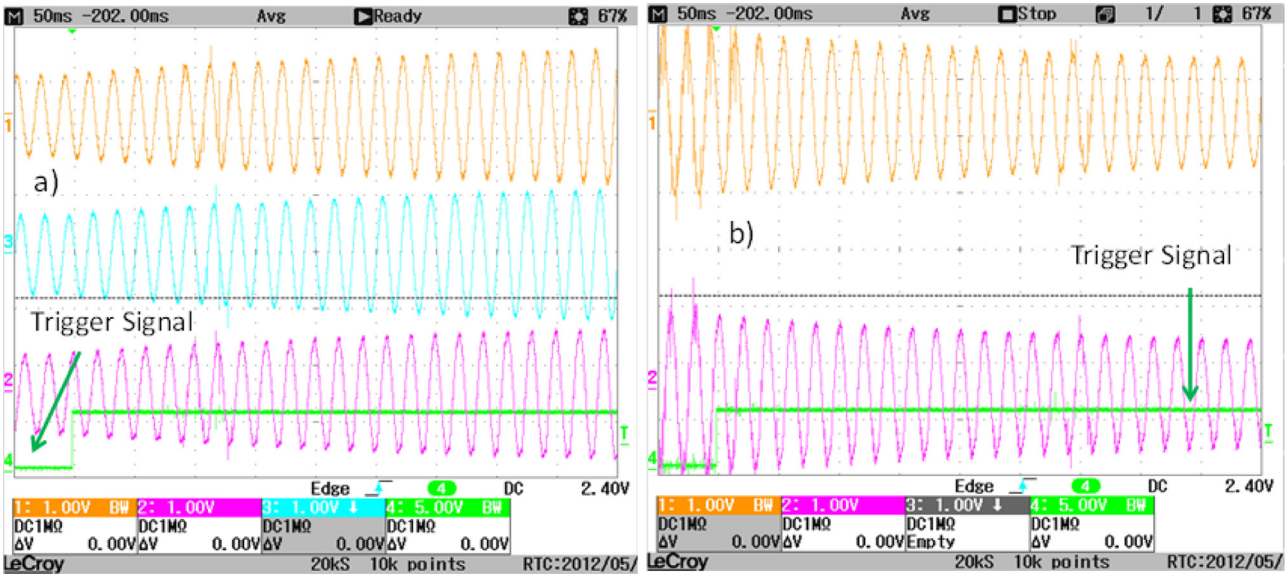

Fig. 16. Dynamic performance of the proposed repetitive controller. (a) Performance for a step-up in the reference voltage. (b) Performance for a step-down in the reference voltage.

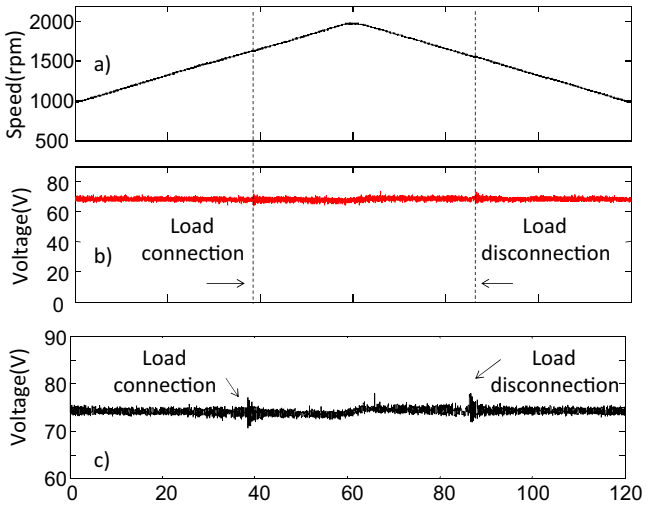

Fig. 17. Performance of the system considering a non-linear load step and frequency variation at the MC input. (a) Permanent magnet machine rotational speed. (b) Magnitude of the load voltage vector. (c) Zoomed view of the load voltage corresponding to the test of (b).

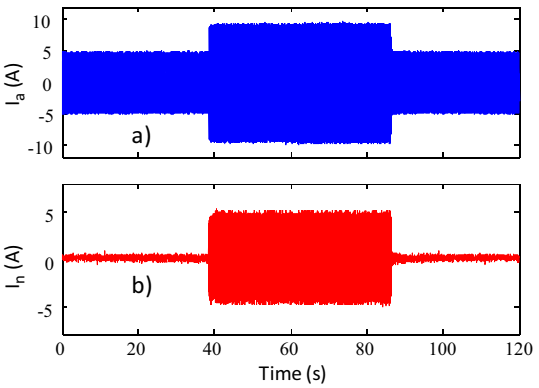

Fig. 18. Unbalanced load current corresponding to the test of Fig. 17. (a) Current step in phase a. (b) Current in the neutral provided by the 4th leg.

Table 1
Summary of the performance for a high-order resonant controller.

Processing time high order resonant controller	≈200 μs
Total harmonic distortion (THD)	>3%
Settling time for a step change in the input reference	5–8 cycles (50 Hz)

Table 2
Summary of the performance for the proposed repetitive controller.

Processing time repetitive controller	≈50 μs
Total harmonic distortion	<2.5%
Settling time for a step change in the input reference	18 cycles (50 Hz)

The experimental results shown in Figs. 13 and 14 demonstrate the good performance achieved in steady state operation with the proposed repetitive controller. The load is strongly non-linear because of the half-wave rectification in phase *a*. The load current is shown in the bottom trace of Fig. 15.

The dynamic performance of the repetitive controller is shown in Fig. 16. Here, the digital oscilloscope is operated in single-shot mode with a trigger signal obtained from one of the D/A converters controlled by the FPGA board. Fig. 16a shows a step up in the reference voltage from 35 V to 70 V. The repetitive control system drives the load voltage to the new reference voltage in about 18cycles. Fig. 16b shows the step down performance. In this case the reference signal is changed from 70 V to 35 V with a similar performance to that obtained from Fig. 16a. For the results in Fig. 16 the non-linear load was unchanged from that used for Figs. 13 and 14.

Performance of the repetitive controller considering step variations in the load and variable frequency operation at the MC input is shown in Fig. 17. In this case, the MC is fed from the permanent magnet generator. The rotational speed is increased from $\omega_r = 1000$ rpm to $\omega_r = 2000$ rpm in 60 s (corresponding to an MC input frequency variation of ≈66 Hz to ≈130 Hz). At $t = 60$ s the rotational speed is decreased back to 1000 rpm (see Fig. 17a). Initially the MC is feeding a resistive balanced load of ≈15 Ω in each phase. At $t \approx 38$ s an additional 15 Ω resistor is connected in parallel with one of the phases. This unbalanced load is disconnected at $t \approx 86$ s.

Fig. 17b shows the magnitude of the load voltage (calculated from the α–β–γ components). Notice that the load voltage is well regulated despite the input frequency variation and the load step at the output. Fig. 17c shows a zoomed view of Fig. 17b. Notice that the load steps produce a dip and an overshoot of less than 5 V in the output voltage. In Fig. 18a the unbalanced load step in the (phase a) current is shown. Notice that the zero sequence current is circulating through the neutral connection provided by the 4th leg of the MC (see Fig. 18b).

6. Discussion

It has been shown in this section that the repetitive control system, proposed for the variable speed generation topology of Fig. 3, has good performance. For the same generation topology the authors have implemented high order resonant controllers whose performance is reported in [17]. A summary of the performance is presented, for the same operating conditions in Tables 1 and 2.

The resonant controller with six gain peaks, reported in [17] achieved a THD of 3% (with a non-linear load identical to that used in this work noting that dc components are not considered for the calculation of the THD) but requires a processing time of about 200 μS in a Texas Instrument DSK6713 DSP. The repetitive controller discussed in this work produces more than six resonant peaks (as shown in Fig. 10) and can be implemented in just 50 μS of processing time. Because the repetitive controller has more high gain peaks it can reduce the THD to about 2.3–2.5%. However the dynamic response of a high order resonant controller is faster, with a settling times of about five cycles for step changes in the output voltage (typically the dynamic response is dependent on the size of the output filter capacitor). Both, repetitive and resonant controllers have a relatively good response to step changes in the load. The main advantage of a repetitive controller is in the reduced processing time producing lower THD in steady state. Moreover, step changes in the load voltage are unlikely for a typical variable speed diesel generation system, which is mostly subjected to fast load changes. As shown in this paper the proposed repetitive control system has a good dynamic response for unbalanced linear/non-linear load step variations.

As discussed in the introduction, the MC has many advantages when compared to voltage source inverters in term of size and reliability. However, as mentioned before, there are no energy storage components in the matrix converter. Therefore the MC input current has some harmonic distortion when the converter is feeding unbalanced distorted loads. This is shown in Fig. 19. The output current corresponds to that shown in Fig. 14b. The input current (see Fig. 19b) has some harmonic distortion with a total THD of about 22%. This THD value is the same for all the input currents.

As stated before, the permanent magnet generator is capable of operating with a relatively high current distortion. However, there

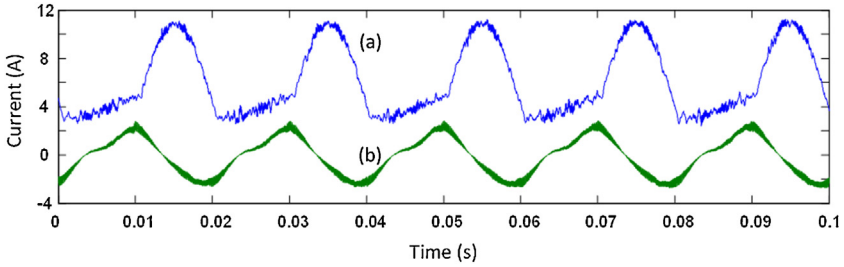

Fig. 19. Matrix converter current for non-linear operation. (a) MC output current. (b) MC input current.

Table 3
Parameters of the experimental rig.

Parameter of the MC input filter	$L_f = 0.625$ mH, $C_f = 2$ μF
Parameters of the MC output filter	$L = 2.5$ mH, $C = 40$ μF
MC commutation method	4-Step commutation method, $T = 0.7$ μS in each step
MC switching frequency	10 kHz
MC fundamental output frequency	50 Hz
MC fundamental input frequency	Tested in an operating range from 50 Hz to 130 Hz
MC nominal power	≈3 kW for a 380 V line to line input voltage
Number of poles permanent magnet generator	8
PMG nominal speed and power	2000 rpm, 5 kW
Prime mover	Cage machine, 2 poles, 2910 rpm, 5 kW nominal power

will ultimately be a limit to the degree of unbalance/distortion that can be allowed in the load fed by the 4-leg MC.

7. Conclusions

This paper has presented the application of a repetitive control system to a 4-leg matrix converter power supply. The controller is designed to eliminate the harmonic distortion from a non-linear load connected at the 3×4 MC outputs. Because of the periodic nature of the distortion, a repetitive controller can be used to advantage for improving the THD at the MC output voltage. The proposed control system has good performance in steady-state and is able to deal with distortion introduced by highly non-linear loads. System performance for step changes in the reference voltages has been presented, illustrating an acceptable dynamic response. Controller performance for step changes in load has also been presented, showing good regulation of the output voltage regardless of the generator speed. The computational burden of the repetitive controller is low and operation with high switching frequency and reduced THD is easily achievable.

The aim of this work was to obtain a low load-voltage THD, with a reduced computational burden and an appropriate dynamic response. According to the experimental result presented in this paper, this aim has been achieved.

Acknowledgements

This work was partially funded by Fondecyt Chile, Grant Nr. 1110984 and CONICYT/FONDAP/15110019. Travel expenses of a British researcher to the University of Chile were partially funded by the academic link REDENERG-0002, Conicyt Chile.

Appendix A. Appendix

See Table 3

References

[1] L.M. Tolbert, W.A. Peterson, T.J. Theiss, M.B. Scudiere, Gen-sets, IEEE Industry Applications Magazine 9 (2003) 48–54.
[2] D. Arap, Modelling, Simulation, and Performance Analysis of a Hybrid Power System for Mobile Medical Clinic, Univ. of Kassel, Kassel, Germany, 2004 (Ph.D. Thesis).
[3] R. Pena, R. Cardenas, J. Proboste, J. Clare, G. Asher, Wind-diesel generation using doubly fed induction machines, IEEE Transactions on Energy Conversion 23 (2008) 202–214.
[4] S.R.P. Malik, G.S. Hope, Real-time test results with adaptive speed controllers for a diesel prime-mover, IEEE Transactions on Energy Conversion 7 (1992) 499–505.
[5] R. Cardenas, R. Peña, C. Juri, P. Wheeler, J. Clare, Control of a matrix converter for the operation of autonomous systems, Renewable Energy 27 (2012) 1120–1129.
[6] A. Lidozzi, L. Solero, F. Crescimbini, Adaptive direct-tuning control for variable-speed diesel-electric generating units, IEEE Transactions on Industrial Electronics 59 (2012) 2126–2134.
[7] J. Andriulli, Advanced Power Generation Systems for the 21st Century: Market Survey and Recommendations for a Design Philosophy, Oak Ridge National Laboratory, 1999, Tech. Rep.
[8] S.L. Arevalo, P. Zanchetta, P.W. Wheeler, A. Trentin, L. Empringham, Control and implementation of a matrix-converter-based AC ground power-supply unit for aircraft servicing, IEEE Transactions on Industrial Electronics 57 (2010) 2076–2084.
[9] F. Yue, P.W. Wheeler, N. Mason, J.C. Clare, Indirect space vector modulation for a 4-leg matrix converter, in: 2007 IEEE Power Electr. Specialists Conf., IEEE, 2007, pp. 639–645.
[10] R. Cardenas, R. Pena, P. Wheeler, J. Clare, Experimental validation of a space vector modulation algorithm for four-leg matrix converters, IEEE Transactions on Industrial Electronics 58 (2011) 1282–1293.
[11] M. Aten, G. Towers, C. Whitley, P. Wheeler, J. Clare, K. Bradley, Reliability comparison of matrix and other converter topologies, IEEE Transactions on Aerospace and Electronic Systems 42 (2006) 867–875.
[12] T. Friedli, J.W. Kolar, J. Rodriguez, P.W. Wheeler, Comparative evaluation of three-phase AC–AC matrix converter and voltage DC-link back-to-back converter systems, IEEE Transactions on Industrial Electronics 59 (2012) 4487–4510.
[13] T.F. Podlesak, D.C. Katsis, P.W. Wheeler, J.C. Clare, L. Empringham, M. Bland, A 150-kVA vector-controlled matrix converter induction motor drive, IEEE Transactions on Industry Applications 41 (2005) 841–847.
[14] P.W. Wheeler, J.C. Clare, L. Empringham, M. Bland, K.G. Kerris, Matrix converters, IEEE Industrial Applications Magazine 10 (2004) 59–65.
[15] P.W. Wheeler, J. Rodriguez, J.C. Clare, L. Empringham, A. Weinstein, Matrix converters: a technology review, IEEE Transactions on Industrial Electronics 49 (2002) 276–288.
[16] R. Cardenas, C. Juri, R. Pena, J. Clare, P. Wheeler, Analysis and experimental validation of control systems for four-leg matrix converter applications, IEEE Transactions on Industrial Electronics 59 (2012) 141–153.
[17] R. Cardenas, C. Juri, R. Pena, P. Wheeler, J. Clare, The application of resonant controllers to four-leg matrix converters feeding unbalanced or nonlinear loads, IEEE Transactions on Power Electronics 27 (2012) 1120–1129.
[18] R. Costa-Castello, J. Nebot, R. Grino, Demonstration of the internal model principle by digital repetitive control of an educational laboratory plant, IEEE Transactions on Education 48 (2005) 73–80.

[19] T. Friedli, J. Kolar, J. Rodriguez, P. Wheeler, Comparative evaluation of three-phase AC–AC matrix converter and voltage DC-link back-to-back converter systems, IEEE Transactions on Industrial Electronics 59 (2012) 4487–4510.
[20] S. Jiang, D. Cao, Y. Li, J. Liu, F.Z. Peng, T.H.D. Low, Fast transient, and cost-effective synchronous-frame repetitive controller for three-phase UPS inverters, IEEE Transactions on Power Electronics 27 (2012) 2994–3005.
[21] P.C. Loh, Y. Tang, F. Blaabjerg, P. Wang, Mixed-frame and stationary-frame repetitive control schemes for compensating typical load and grid harmonics, IEEE Transactions on Power Electronics 4 (2011) 218–226.
[22] M. Rashed, C. Klumpner, G. Asher, Control scheme for a single phase hybrid multilevel converter using repetitive and resonant control approaches, in: Proc. of the 2011-14th Europ. Conf. On Power Electr. and Appl. (EPE 2011), 2011, pp. 1–13.
[23] X.H. Wu, S.K. Panda, J.X. Xu, Design of a plug-in repetitive control scheme for eliminating supply-side current harmonics of three-phase PWM boost rectifiers under generalized supply voltage conditions, IEEE Transactions on Power Electronics 25 (2010) 1800–1810.
[24] Y. Tzou, I. Member, R. Ou, S. Jung, M. Chang, High-performance programmable AC power source with low harmonic distortion using DSP-based repetitive control technique, IEEE Transactions on Power Electronics 12 (1997) 715–725.
[25] K. Zhou, D. Wang, Digital repetitive controlled three-phase PWM rectifier, IEEE Transactions on Power Electronics 18 (2003) 309–316.
[26] M. Tomizuka, T. Tsao, K. Chew, Analysis and synthesis of discrete-time repetitive controllers, Journal of Dynamic Systems, Measurement, and Control 111 (1989) 353–358.
[27] P.W. Wheeler, P. Zanchetta, J.C. Clare, L. Empringham, M. Bland, D. Katsis, A utility power supply based on a four-output leg matrix converter, IEEE Transactions on Industry Applications 44 (2008) 174–186.
[28] O. Carranza, E. Figueres, G. Garcerá, L.G. González, A. Juan, D.D. Bátiz, et al., Peak current mode control of a boost rectifier with low distortion of the input current for wind power systems based on permanent magnet synchronous generators keywords boost rectifier in DCM, in: 13th Europ. Conf. on Power Electr. and Appl. (EPE09), 2009, pp. 1–10.
[29] K. Ogata, Modern Control Engineering, 5th ed., Prentice Hall, 2010, Englewood Cliffs NJ 07632.
[30] Y. Cho, Jih-Sheng Lai, Digital plug-in repetitive controller for single-phase bridgeless PFC converters, IEEE Transactions on Power Electronics 28 (2013) 165–175.
[31] B. Zhang, D. Wang, K. Zhou, Y. Wang, Linear phase lead compensation repetitive control of a CVCF PWM inverter, IEEE Transactions on Industrial Electronics 55 (2008) 1595–1602.
[32] C. Rech, H. Pinheiro, H.A. Grundling, H.L. Hey, J.R. Pinheiro, Comparison of digital control techniques with repetitive integral action for low cost PWM inverters, IEEE Transactions on Power Electronics 18 (2003) 401–410.
[33] D. Casadei, G. Serra, A. Tani, L. Zarri, Matrix converter modulation strategies: a new general approach based on space-vector representation of the switch state, IEEE Transactions on Industrial Electronics 49 (2) (April 2002) 370–381.